ACS Catalysis

Research Article

pubs.acs.org/acscatalysis

Electrocatalytic Hydrogen Production by $[Ni(7P^{Ph}_2N^H)_2]^{2+}$: Removing the Distinction Between Endo- and Exo-Protonation Sites

Houston J. S. Brown, Stefan Wiese, John A. S. Roberts, R. Morris Bullock, and Monte L. Helm*

Center for Molecular Electrocatalysis, Physical Sciences Division, Pacific Northwest National Laboratory, P.O. Box 999, K2-57, Richland, Washington 99352, United States

Supporting Information

ABSTRACT: A new Ni(II) complex, $[Ni(7P^{Ph}_2N^H)_2H]^{3+}$ ($7P^{Ph}_2N^H$ = 3,6-diphenyl-1-aza-3,6-diphosphacycloheptane), has been synthesized, and its electrochemical properties have been reported. The $7P^{Ph}_2N^H$ ligand features an NH, ensuring properly positioned protonated amine groups (N–H^+) for electrocatalysis, regardless of whether protonation occurs exo or endo to the metal center. The compound is an electrocatalyst for H_2 production in the presence of organic acids (pK_a range 10–13 in CH_3CN), with turnover frequencies ranging from 160 to 780 s^{-1} at overpotentials between 320 and 470 mV, as measured at the potential of the catalytic wave. In stark contrast to $[Ni(P^{Ph}_2N^{R'}_2)_2]^{2+}$ ($P^{Ph}_2N^{R'}_2$ = 3,7-diphenyl-1,5-diaza-3,7-diphosphacyclooctane) and other $[Ni(7P^{Ph}_2N^{R'})_2]^{2+}$ complexes, catalytic turnover frequencies for H_2 production by $[Ni(7P^{Ph}_2N^H)_2]^{2+}$ do not show catalytic rate enhancement upon the addition of H_2O. This finding supports the assertion that $[Ni(7P^{Ph}_2N^H)_2]^{2+}$ eliminates the distinction between the endo- and exo-protonation isomers.

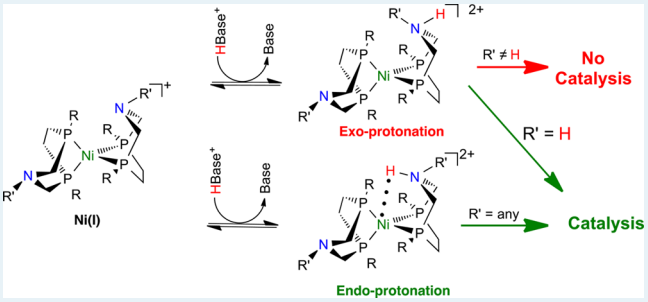

KEYWORDS: *hydrogen production, electrocatalysis, proton relays, pendant amines, nickel complexes, nickel phosphine complexes*

INTRODUCTION

As a clean fuel, H_2 is an ideal storage medium for renewable, sustainable energy technologies.[1−3] The development of molecular complexes for the electrocatalytic production of H_2 has made remarkable progress through the incorporation of design elements present in Nature's catalysts for production and oxidation of H_2—the hydrogenases.[4−8] For example, the active site of [FeFe]-hydrogenase features two iron centers bridged by an azadithiolate cofactor (Figure 1a).[9−11] Mechanistic studies indicate that this pendant amine functionality serves a crucial role in the H_2 production cycle by relaying protons from the surrounding protein matrix to the metal center.[12] The [FeFe]-hydrogenase produces H_2 with amazing efficiency at rates ≥9000 s^{-1} at overpotentials ≤100 mV.[12,13] Achieving such remarkable catalytic performance requires precise delivery of electrons and protons to the active site of the enzyme to form the H–H bond. As such, functional mimics of the [FeFe]-hydrogenase active sites often feature similarly positioned proton relays.[5,14]

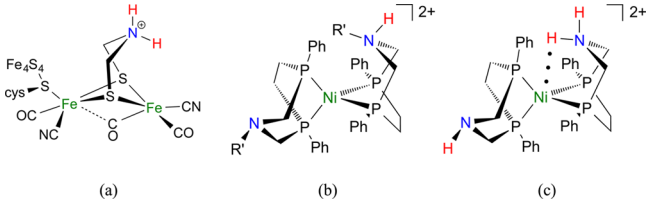

Figure 1. (a) Proposed structure for the active site of the protonated [FeFe]-hydrogenase active site. (b) Exo-protonated Ni(I) isomer of $[Ni(7P^{Ph}_2N^{R'})_2H]^{2+}$. (c) Protonated Ni(I) isomer of $[Ni(7P^{Ph}_2N^H)_2H]^{2+}$.

Efforts in our laboratory have focused on developing first-row-metal complexes (Ni, Co, Fe, and Mn) that contain an amine base in the second coordination sphere for controlling proton movement to/from the metal center.[6,15−20] For example, $[Ni(7P^{Ph}_2N^{Ph})_2]^{2+}$ features positioned pendant amines and catalyzes the production of H_2 at rates >100000 s^{-1}.[21] A related series of $[Ni(7P^{Ph}_2N^{R'})_2]^{2+}$ ($7P^{Ph}_2N^{R'}$ = 3,6-diphenyl-1-aza-3,6-diphosphacycloheptane) catalysts with different aryl substituents on the N atoms illustrates how the basicity of the proton relay can influence the turnover frequency for H_2 production.[22] Although the $[Ni(7P^{Ph}_2N^{R'})_2]^{2+}$ complexes are electrocatalysts for H_2 production, their rates can be limited by kinetically favored exo protonation of the pendant amine (Figure 1b). Computational and mechanistic investigations confirm that catalysis by both $[Ni(P^{Ph}_2N^{R'}_2)_2]^{2+}$ ($P^{Ph}_2N^{R'}_2$ = 3,7-diphenyl-1,5-diaza-3,7-diphosphacyclooctane) and $[Ni(7P^{Ph}_2N^{R'})_2]^{2+}$ requires a protonated amine functionality (N–H^+) positioned endo to the metal center for H_2 production (e.g., Figure 1c).[22−24] Exo protonation, forming an (N–H^+) bond away from the metal center, limits the rate of catalysis through the formation of less productive catalytic intermediates. The active

Received: July 28, 2014
Revised: February 9, 2015
Published: February 11, 2015

DOI: 10.1021/cs502132y
ACS Catal. 2015, 5, 2116−2123

Scheme 1. Synthesis of *meso*- and *rac*- $7P^{Ph}{}_2N^{CHPh_2}$ and $[Ni(7P^{Ph}{}_2N^{CHPh_2})_2](BF_4)_2$

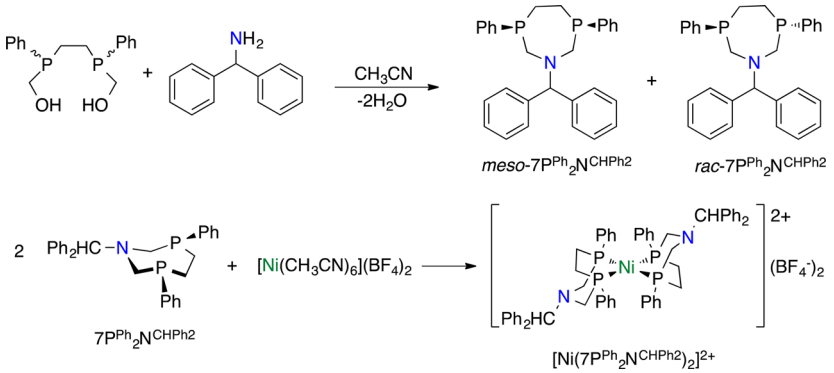

site of [FeFe]-hydrogenase has a more constrained environment due to the surrounding protein matrix that helps minimize undesirable conformations. The proton relay in the natural system also features a secondary amine; protonation in either an exo or endo position results in an $N-H^+$ functionality adjacent to the metal center (Figure 1a). Following Nature's lead, we report the synthesis and electrochemical behavior of a new $[Ni(7P^{Ph}{}_2N^{H})_2]^{2+}$ catalyst designed to eliminate the exo-protonation limitation by incorporating a secondary amine into the ligand backbone (Figure 1c).

RESULTS

Synthesis and Characterization of $[Ni(7P^{Ph}{}_2N^{CHPh_2})_2](BF_4)_2$ and $[Ni(7P^{Ph}{}_2N^{H})_2H](BF_4)_3$. The synthesis of $[Ni(7P^{Ph}{}_2N^{H})_2H]^{3+}$ was accomplished through formation and conversion of the protected $[Ni(7P^{Ph}{}_2N^{CHPh_2})_2](BF_4)_2$ ($CHPh_2$ = diphenylmethyl) complex.[25] The $7P^{Ph}{}_2N^{CHPh_2}$ ligand was synthesized by addition of benzhydrylamine to 1,2-bis(hydroxymethylphenylphosphino)-ethane in CH_3CN (Scheme 1). The desired 1-aminodiphenylmethyl-3,6-diphenyl-1-aza-3,6-diphosphacycloheptane ligand was isolated as a 1:1 mixture of the *rac* and *meso* stereoisomers, as reported for other $7P^{Ph}{}_2N^{R'}$ ligands (Scheme 1) and fully characterized by multinuclear NMR spectroscopy and elemental analysis.[22,26] The addition of 2 equiv of $7P^{Ph}{}_2N^{CHPh2}$ to a solution of $[Ni(CH_3CN)_6](BF_4)_2$ shows the formation of $[Ni(7P^{Ph}{}_2N^{CHPh_2})_2]^{2+}$ as determined by $^{31}P\{^1H\}$ NMR spectroscopy (Scheme 1). In addition to the desired homoleptic monometallic complex, the formation of oligomeric metal complexes is suggested by broad resonances in the $^{31}P\{^1H\}$ NMR spectrum of the reaction mixture, as previously observed in other $[Ni(7P^{Ph}N^{R})_2]^{2+}$ syntheses.[21,22] The $[Ni(7P^{Ph}{}_2N^{CHPh_2})_2](BF_4)_2$ complex is separated from oligomeric products by recrystallization from CH_2Cl_2/Et_2O, yielding a pure, red crystalline solid in 73% yield. The $[Ni(7P^{Ph}{}_2N^{CHPh2})_2](BF_4)_2$ complex was fully characterized by NMR spectroscopy, elemental analysis, and single-crystal X-ray analysis.

X-ray-quality crystals of $[Ni(7P^{Ph}{}_2N^{CHPh_2})_2](BF_4)_2$ were grown by slow diffusion of Et_2O into a saturated CH_3CN solution. The $[Ni(7P^{Ph}{}_2N^{CHPh_2})_2]^{2+}$ dication crystallizes with the two BF_4^- ions interacting weakly with the metal center, resulting in a pseudo-octahedral structure around the Ni center, with Ni···F distances of 3.00 Å (Figure 2). The structure confirms that the $7P^{Ph}{}_2N^{CHPh_2}$ ligands coordinate as diphosphine chelates to give a distorted-square-planar geometry, with the four Ni–P bond distances being nearly equal, ranging from 2.18 to 2.20 Å. The P–Ni–P bite angle for each of the diphosphine ligands is 79.12°, smaller than the 82–84° typically

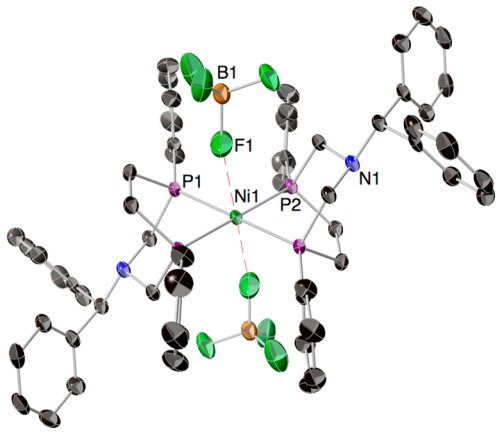

Figure 2. X-ray crystal structure of $[Ni(7P^{Ph}{}_2N^{CHPh2})_2](BF_4)_2$. Thermal ellipsoids are shown at the 50% probability level. Hydrogen atoms have been omitted for clarity.

observed for the P–Ni–P bite angle in $[Ni(P^R{}_2N^{R'}{}_2)_2]^{2+}$ complexes but in the normal range for previously reported $[Ni(7P^{Ph}{}_2N^{R'})_2]^{2+}$ complexes.[21,22,27,28] The two six-membered rings containing the pendant amines are trans to each other with respect to the metal center and are in chair conformations (Figure 1).[22,27,28] The $^{31}P\{^1H\}$ NMR spectra of $[Ni(7P^{Ph}{}_2N^{CHPh_2})_2]^{2+}$ at room temperature in CH_3CN show the presence of conformational isomers resulting from the position of the pendant amines, either on the same side (up–up), or on opposite sides (up–down) of the square-planar nickel complex. Although the crystal structure of the $[Ni(7P^{Ph}{}_2N^{CHPh_2})_2]^{2+}$ complex shows a single isomer, previous studies on the related $[Ni(7P^{Ph}{}_2N^{R'})_2]^{2+}$ complexes show the isomers to be in exchange at room temperature in CH_3CN solutions.[21,22] Complete crystallographic information on $[Ni(7P^{Ph}{}_2N^{CHPh_2})_2](BF_4)_2$ is contained in the Tables S1 and S2 in the Supporting Information.

Removal of the diphenylmethyl protecting group on the amines of $[Ni(7P^{Ph}{}_2N^{CHPh_2})_2]^{2+}$ can be achieved through addition of a slight excess (~5%) of $HBF_4{\cdot}Et_2O$, resulting in a solid orange precipitate of $[Ni(7P^{Ph}{}_2N^{H})_2H](BF_4)_3$ in 65% yield.[25] The product was characterized by ^1H and $^{31}P\{^1H\}$ NMR spectra, which showed multiple conformational isomers in CD_3CN solutions as shown and discussed in the Figures S1 and S2 in the Supporting Information. A satisfactory elemental analysis for the compound was obtained, confirming the stoichiometry, but separation of the conformational isomers or suitable crystals for X-ray diffraction was not accomplished. An alternative acid deprotection route using trifluoroacetic acid

DOI: 10.1021/cs502132y
ACS Catal. 2015, 5, 2116–2123

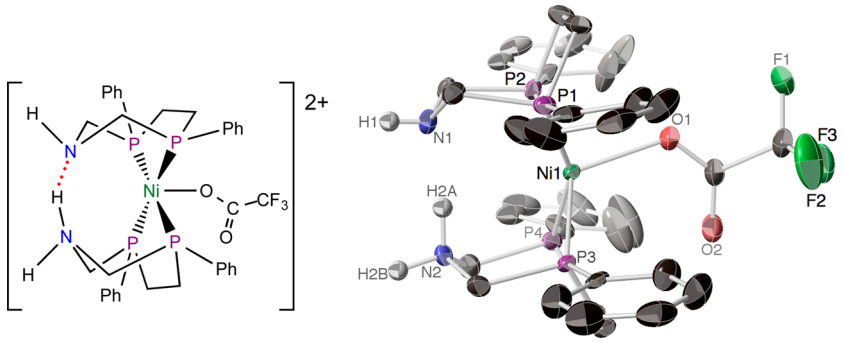

Figure 3. Structural drawing (left) and X-ray crystal structure (right) of $[Ni(CF_3COO)(7P^{Ph}_2N^H)_2H]^{2+}$. The BF_4^- counterions, CH_2Cl_2 solvent molecules, and H atoms have been omitted for clarity. Thermal ellipsoids are shown at the 50% probability level.

also yielded a $^{31}P\{^1H\}$ NMR spectrum of the reaction mixture that is consistent with multiple conformational isomers. Deprotection by this route leads to fractional crystallization of a single conformational isomer that allowed for structural analysis of $[Ni(CF_3COO)(7P^{Ph}_2N^H)_2H](BF_4)_2$ (Figure 3). The compound crystallizes with a $[Ni(CF_3COO)(7P^{Ph}_2N^H)_2H]^{2+}$ dication, two noncoordinating BF_4^- anions, and two CH_2Cl_2 solvent molecules in the unit cell. The complex has a five-coordinate Ni(II) center, with four phosphorus atoms and one coordinating oxygen atom from a CF_3COO^- anion. The conformational isomer that crystallized contained two P−N−P six-membered rings arranged in boat conformations on the same side of the Ni(II) center (up−up conformation) with a proton "pinched" between adjacent N atoms. Crystallographic data and selected bond angles and distances are provided in the Tables S3 and S4 in the Supporting Information.

NMR Spectroscopic Studies of $[Ni(CF_3COO)(7P^{Ph}_2N^H)_2H](BF_4)_2$ in CD_3CN. To gain insight into the NMR spectra of $[Ni(7P^{Ph}_2N^H)_2H]^{3+}$ that show multiple conformational isomers, the fractionally crystallized single isomer used for structural analysis of $[Ni(CF_3COO)(7P^{Ph}_2N^H)_2H](BF_4)_2$ was studied in CD_3CN. The $^{31}P\{^1H\}$ NMR spectrum of the complex shows a single resonance attributed to the up−up conformational isomer that shifts between 58.7 and 60.7 ppm as the temperature was decreased. The ^{19}F NMR spectrum of the complex shows resonances at −85 and −153 ppm for the Ni(II)-bound CF_3COO^- and BF_4^- anions, respectively. The ^1H NMR spectrum of $[Ni(CF_3COO)(7P^{Ph}_2N^H)_2H]^{2+}$ shows the anticipated resonances for methylene and phenyl protons; however, no peaks for N−H protons were observed at room temperature. At −40 °C, two additional resonances become apparent at 6.2 and 11.2 ppm that integrate as approximately 2:1 (Figure S3 in the Supporting Information). The two-proton resonance centered at 6.2 ppm is assigned to the N−H protons pointing exo to the metal center, and the downfield one-proton resonance at 11.2 ppm is assigned to the "pinched" endo N−H proton. Similar chemical shifts in the low-temperature ^1H NMR spectrum of $[Ni(7P^{Ph}_2N^H)_2H]^{3+}$ were also observed (Figures S1 and S2 in the Supporting Information). To avoid possible complications from trifluoroacetate binding during electrocatalytic hydrogen production, $[Ni(7P^{Ph}_2N^H)_2H]^{3+}(BF_4)_3$ was used in all electrochemical and electrocatalytic studies described below.

Cyclic Voltammetry Studies of $[Ni(7P^{Ph}_2N^H)_2H]^{3+}$. Cyclic voltammograms of $[Ni(7P^{Ph}_2N^H)_2H]^{3+}$ show two irreversible redox events at −1.05 and −1.16 V, which become a single reversible wave upon treatment with triethylamine (Figure 4). The $E_{1/2}$ value of this reversible wave is −1.13 V, which is

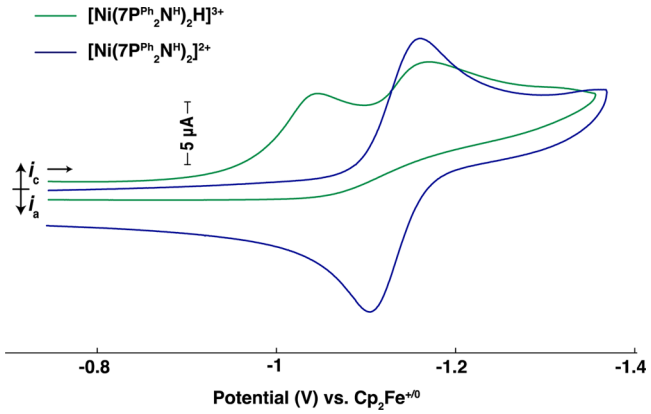

Figure 4. Cyclic voltammograms of 1.0 mM $[Ni(7P^{Ph}_2N^H)_2H]^{3+}$ (green) and 1.0 mM $[Ni(7P^{Ph}_2N^H)_2]^{2+}$ (blue) formed in solution by the addition of 4.2 mM NEt_3 to 1.0 mM $[Ni(7P^{Ph}_2N^H)_2H]^{3+}$. Conditions: 0.1 M Bu_4NPF_6 in CH_3CN at 22 °C, scan rate 1 V s^{-1}.

consistent with the irreversible wave observed with an E_p value of −1.16 V. The first irreversible wave may be due to the reduction of the protonated species, which may then eliminate H_2 through a bimolecular pathway. To verify the additional reduction event, a controlled-potential electrolysis experiment was performed, resulting in a total of 3 equiv of electrons passed for each 1 equiv of metal complex (Table S5 in the Supporting Information). The observed three electrons per nickel complex is consistent with production of 1/2 equiv of H_2 per complex, in addition to the two-electron reduction of Ni(II) to Ni(0). A plot of the cathodic peak current (i_p) versus the square root of the scan rate shows a linear correlation, implying diffusion-controlled electrochemical events. The absence of two clear Ni(II/I) and Ni(I/0) features indicates that the second redox process is likely occurring at or positive of the first redox potential. At all scan rates studied, the difference in the potentials of the cathodic and anodic peak potentials (ΔE_p) for this feature are less than the ΔE_p value observed for the $Cp_2Fe^{+/0}$ one-electron couple, consistent with a two-electron redox event. For example, the ΔE_p value at a scan rate of 1 V/s for the overlapping Ni(II/I) and Ni(I/0) processes was measured to be 55 mV, under conditions where the ΔE_p value of $Cp_2Fe^{+/0}$ is 71 mV. The difference in the ΔE_p value of $Cp_2Fe^{+/0}$ in comparison to that of in situ generated $[Ni(7P^{Ph}_2N^H)_2]^{2+}$ was also confirmed with square wave voltammetry (Figure S4 in the Supporting Information). The two-electron nature of the reversible wave was also confirmed with a controlled-potential electrolysis experiment, as described in Table S5. The observation of a two-electron overlapping

DOI: 10.1021/cs502132y
ACS Catal. 2015, 5, 2116−2123

process in the cyclic voltammetry of in situ generated $[Ni(7P^{Ph}_2N^H)_2]^{2+}$ is consistent with the previously observed and simulated data for other members of the $[Ni(7P^{Ph}_2N^{R'})_2]^{2+}$ family.[21,22]

Electrocatalytic Hydrogen Production. Addition of an acid to in situ generated $[Ni(7P^{Ph}_2N^H)_2]^{2+}$ results in a significant current enhancement near the two-electron Ni(II/0) couple, indicating production of H_2 (Figure 5). Values for k_{obs} (turnover frequency, TOF) were determined using eq 1, where

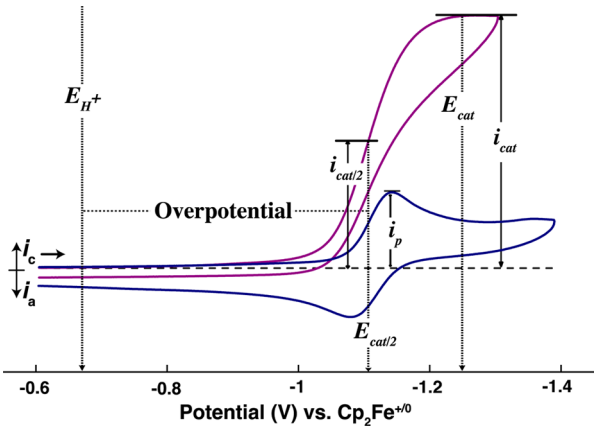

Figure 5. Cyclic voltammograms illustrating the experimental parameters used for calculating TOF and overpotential: (blue trace) 1 mM $[Ni(7P^{Ph}_2N^H)_2H]^{3+}$ and 3 mM NEt_3; (purple trace) after the addition of 7 mM 2,6-di-*tert*-butylpyridinium tetrafluoroborate and 7 mM 2,6-di-*tert*-butylpyridine. Conditions: 0.1 M Bu_4NPF_6 in CH_3CN, scan rate 1 V s^{-1}.

$$k_{obs} = 1.94\ V^{-1} \times \nu \left(\frac{i_{cat}}{i_p} \right)^2 \quad (1)$$

ν is the scan rate, i_p defines the noncatalytic one-electron peak current (obtained from a simulation of experimental data that accounts for the two-electron Ni(II/0) redox couple; Figure S5 and Table S6 in the Supporting Information), and i_{cat} is the scan-rate independent catalytic current measured at the point where the catalytic wave first plateaus, as defined by a point where the second derivative first reaches a constant value (Figure 5; scan rate dependence shown in Figure S6).[29,30] The overpotentials are calculated as the difference between the equilibrium potential for proton reduction (E_{H^+}) and the potential of the catalytic wave, $E_{cat/2}$, defined as the potential at half the catalytic current ($i_{cat/2}$) used to calculate the TOF (Figure 5 and eq 2). The E_{H^+} is determined as a function of

$$\text{overpotential} = |E_{H^+} - E_{cat/2}| = \left| \left(E^\circ_{H^+} + \frac{RT}{nF} \ln \frac{[H^+]}{P_{H_2}} \right) - (E_{cat/2}) \right| \quad (2)$$

proton concentration and H_2 pressure using the Nernst equation (eq 2). Using a value of $E^\circ_{H^+} = -0.028$ V and the conditions used in this study (T = 298 K, 1/1 acid/base buffer solution, as suggested by Helm and Appel to ensure consistent and accurate reporting of rate and overpotential data), eq 2 can be simplified to eq 3, where the pK_a value is that of the acid in CH_3CN.[31,32]

$$\text{overpotential} = |(-0.028\ V - 0.05916\ V \times pK_a) - (E_{cat/2})| \quad (3)$$

Although the ^1H NMR spectrum of $[Ni(7P^{Ph}_2N^H)_2H]^{3+}$ shows the presence of a pinched endo N−H proton at low temperature (Figure S2 in the Supporting Information), this species is likely present only with strong acids (HBF_4) capable of protonating the Ni(II) complex. After in situ generation of $[Ni(7P^{Ph}_2N^H)_2]^{2+}$, the acids used in this study are too weak to protonate the Ni(II) complex. The proposed catalytic mechanism requires reduction of the complex before the first protonation event, substantiated by the *absence* of positive shift in the $E_{cat/2}$ potential relative to the Ni(II/0) couple (Figure 5). This change in oxidation state is accompanied by a change in conformation around the metal center from square planar to tetrahedral.[33] The positions of the pendant amines around a tetrahedral Ni(I) or Ni(0) complex preclude the ability to pinch a proton between the two amines during the catalytic process.

The TOFs and overpotentials for electrocatalytic H_2 production using four 1:1 buffered solutions with pK_a values between 10 and 13 were determined (Table 1): 2,6-di-*tert*-butyl-4-methylpyridinium tetrafluoroborate (12.8), anisidinium tetrafluoroborate (11.9), 2,6-di-*tert*-butylpyridinium tetrafluoroborate (11.4), and anilinium tetrafluoroborate (10.62).[34,35] The use of a 1/1 buffered solution, rather than pure acid, was used to ensure that the concentration of the bulk solution more accurately reflects that at the electrode surface. Buffered solutions with pK_a values below 10 result in decomposition of the complex, and no catalysis was observed using buffered solutions with pK_a values above 13, presumably because the acid is too weak to protonate the complex. In a typical experiment, aliquots of the 1/1 buffered solution were added until no further current enhancement was observed (e.g., Figure 6 and Figures S7−S14 in the Supporting Information). Catalytic currents measured for all four buffered solutions show a concentration dependence at low buffer concentrations but become independent of concentration at higher concentrations, as illustrated in the plot of i_{cat}/i_p versus [buffered acid] (Figure 7 and Figures S7−14). Addition of water to these solutions showed no significant change in the i_{cat}/i_p values. Under these conditions catalysis is pseudo zero-order with respect to acid concentration, resulting in an accurate measure of TOFs (k_{obs}) that range between 160 and 780 s^{-1} with overpotentials of 320−470 mV.

Table 1. Summary of TOFs and Ooverpotentials for H_2 Production by in Situ Generated $[Ni(7P^{Ph}_2N^H)_2]^{2+}$ Determined for 1/1 Buffered Solutions of Four Different Acids

acid (pK_a^{MeCN})	TOF (s^{-1})	[buffer] (mM)	overpotential (mV)
2,6-di-*tert*-butyl-4-methylpyridinium tetrafluoroborate (12.8)	160	47	320
anisidinium tetrafluoroborate (11.86)[34]	710	9.1	410
2,6-di-*tert*-butylpyridinium tetrafluoroborate (11.4)[35]	220	17	410
anilinium tetrafluoroborate (10.62)[34]	780	20	470

For comparison, the catalytic H_2 production by $[Ni(P^{Ph}_2N^{Ph}_2)_2]^{2+}$ and $[Ni(7P^{Ph}_2N^{Ph})_2]^{2+}$ using 1/1 buffered solutions of 2,6-di-*tert*-butylpyridinium and anilinium was explored.

DOI: 10.1021/cs502132y
ACS Catal. 2015, 5, 2116−2123

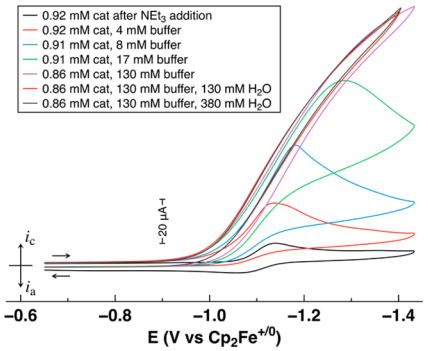

Figure 6. Cyclic voltammograms of in situ generated $[Ni(7P^{Ph}{}_2N^H)_2]^{2+}$ (0.9 mM) in the absence of buffer (black trace) and with varying concentrations of buffered acid (acid = anilinium tetrafluoroborate) and H_2O in acetonitrile (0.1 M Bu_4NPF_6). Scan rate ν = 1 V/s.

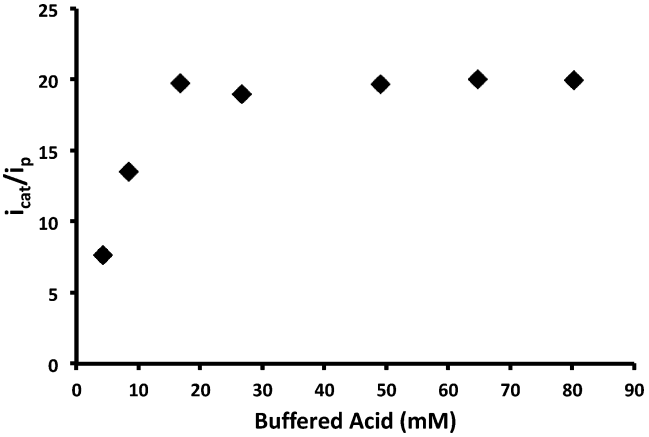

Figure 7. Plot of i_{cat}/i_p vs with varying concentration of buffered acid (acid = anilinium tetrafluoroborate) in acetonitrile (0.1 M Bu_4NPF_6). Scan rate ν = 1 V/s, $[Ni(7P^{Ph}{}_2N^H)_2](BF_4)_2$ (0.9 mM).

Only $[Ni(7P^{Ph}{}_2N^{Ph})_2]^{2+}$ using a 1/1 anilinium/aniline buffered solution showed a current enhancement consistent with catalytic H_2 production (Figures S15 and S16 in the Supporting Information). The TOF in the presence of 90 mM buffered anilinium was determined to be 68 s^{-1}. Addition of small amounts of water (330 mM) resulted in a TOF of 96 s^{-1}. The observation of an increase in rate upon the addition of water to anilinium acids is consistent with previously reported $[Ni(P^{Ph}{}_2N^{C6H4X}{}_2)_2]^{2+}$ complexes.[27]

To confirm the production of H_2, a controlled-potential coulometry experiment was performed using $[Ni(7P^{Ph}{}_2N^H)_2H](BF_4)_3$. By measuring the amount of H_2 produced using gas chromatography, the current efficiency was determined to be 95 ± 5% from the average of three experiments, with calculated turnover numbers of 9, 14, and 19, confirming the selective catalytic production of H_2 (Table S7 in the Supporting Information).

DISCUSSION

The in situ generated $[Ni(7P^R{}_2N^H)_2]^{2+}$ complex is an electrocatalyst for H_2 production in CH_3CN in the presence of a series of organic acids, with TOFs ranging from 160 to 780 s^{-1} and overpotentials between 320 and 470 mV. Previous H_2 production electrocatalytic studies of the $[Ni(7P^{Ph}{}_2N^{R'})_2]^{2+}$ family of complexes were conducted using $[(DMF)H]^+$ (pK_a = 6.1 in MeCN) as the acid.[36,37] Unfortunately, the presence of excess acid with pK_a values <10 leads to decomposition of $[Ni(7P^{Ph}{}_2N^H)_2H]^{3+}$, preventing direct TOF comparisons to other members of this family. Despite this limitation, the observed rates allow for two key conclusions: (1) catalysis by in situ generated $[Ni(7P^R{}_2N^H)_2]^{2+}$ is slower when bulkier acids and increasing pK_a values are employed as the proton source and (2) unlike previously reported $[Ni(7P^{Ph}{}_2N^{R'})_2]^{2+}$ and $[Ni(P^R{}_2N^{R'}{}_2)_2]^{2+}$ catalysts, catalysis by $[Ni(7P^R{}_2N^H)_2]^{2+}$ shows no catalytic rate enhancement in the presence of small amounts of water.

In H_2 production electrocatalyzed by in situ generated $[Ni(7P^R{}_2N^H)_2]^{2+}$, the TOFs in the presence of anilinium acids are more than three times faster than the TOFs in the presence of the more sterically bulky pyridinium acids, regardless of their relative pK_a values (Table 1). The slower rates observed with catalysis using the bulky acids are attributed to slower protonation of the complex. A second trend in the rates of catalysis by in situ generated $[Ni(7P^{Ph}{}_2N^H)_2]^{2+}$ may indicate that acids with lower pK_a values result in faster TOFs. For example, catalysis in the presence of 2,6-di-*tert*-butylpyridinium (pK_a = 11.4) was observed to be 30% faster than catalysis using 2,6-di-*tert*-butyl-4-methylpyridinium (pK_a = 12.8). Previous work on the $[Ni(7P^{Ph}{}_2N^{R'})_2]^{2+}$ family demonstrated that matching the pK_a value of the exogenous acid to that of the protonated pendant amine of the reduced Ni(I) complexes provides the optimal conditions for catalytic TOFs.[22] In catalysis by in situ generated $[Ni(7P^{Ph}{}_2N^H)_2]^{2+}$, acids with a lower pK_a value would likely result in faster TOFs, as they will more closely match the free energies of the protonated intermediates in the catalytic cycle.

To allow for a more direct catalytic comparison, the TOF of H_2 production by $[Ni(7P^{Ph}{}_2N^{Ph})_2]^{2+}$ with a 1/1 anilinium buffer was determined to be 68 s^{-1}, over 1 order of magnitude slower than that of in situ generated $[Ni(7P^{Ph}{}_2N^H)_2]^{2+}$. This drastic difference in rates is likely the result of two effects. First, protonation $[Ni(7P^{Ph}{}_2N^{Ph})_2]^+$ can lead to either exo or endo Ni(I) species (Figure 1). With sterically larger acids, protonation to form the less productive exo isomer is more likely than protonation at the more sterically crowded endo position. Second, protonation of the less basic pendant amine of $[Ni(7P^{Ph}{}_2N^{Ph})_2]^+$ will be less favored than protonation of in situ generated $[Ni(7P^{Ph}{}_2N^H)_2]^+$ by a weak acid such as anilinium, resulting in a slower rate of catalysis. Additionally, the shape of the catalytic waves observed in H_2 production with in situ generated $[Ni(7P^{Ph}{}_2N^H)_2]^+$ in comparison to $[Ni(7P^{Ph}{}_2N^{Ph})_2]^+$ indicated electron transfer may also play a role in determining the rate. This comparison highlights the importance of delivering the proton to the correct position on the catalytic structure *and* matching the pK_a of the proton source to that of the protonated pendant amines.

Previous complexes of the $[Ni(P^{Ph}{}_2N^R{}_2)_2]^{2+}$ and $[Ni(7P^{Ph}{}_2N^{R'})_2]^{2+}$ families show dramatic catalytic improvement in the presence of water.[22,27] For example, the TOF for H_2 production by $[Ni(7P^{Ph}{}_2N^{Ph})_2]^{2+}$ with buffered anilinium was found to increase by 40% upon the addition of small amounts of water, from 68 to 92 s^{-1} (Figure S15 in the Supporting Information). This is in stark contrast to catalysis by $[Ni(7P^{Ph}{}_2N^H)_2]^{2+}$, where no catalytic rate enhancement is observed upon addition of H_2O to the catalytically active solutions. The observation of water-induced current enhancements in the $[Ni(7P^{Ph}{}_2N^{R'})_2]^{2+}$ family has been associated with the protonation of the Ni(I) species in the catalytic cycle (Figure 8). Computational and experimental data identify this

DOI: 10.1021/cs502132y
ACS Catal. 2015, 5, 2116−2123

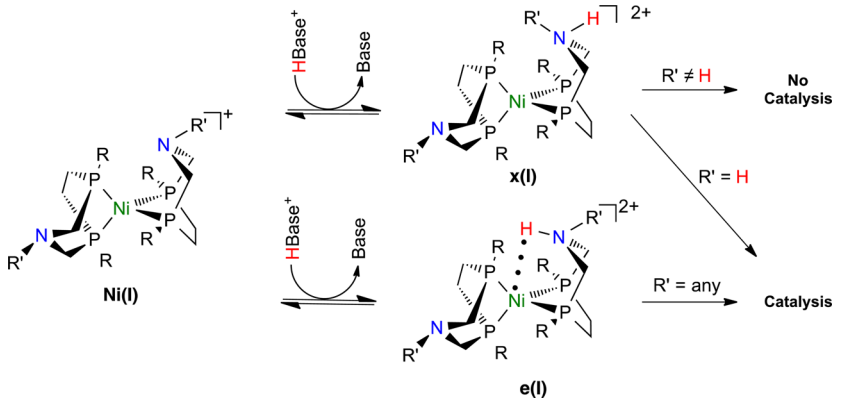

Figure 8. Proposed mechanism for the first protonation step of the mechanism for H_2 production by $[Ni(7P^R_2N^{R'})_2]^{2+}$ type catalysts.

step as rate determining and a branch point in the catalytic cycle, with exo protonation (**x(I)**; Figure 8) slowing the catalytic process (for the complete catalytic cycle, see Figure S17 in the Supporting Information). Water-induced current enhancements are attributed to lower kinetic barriers for endo protonation (**e(I)**; Figure 8); by acting as proton relays, H_2O molecules are hypothesized to provide improved access to congested areas around the metal's primary coordination sphere.[21,27] In the case of protonation of $[Ni(7P^{Ph}_2N^H)_2]^+$, access to protonation of the endo site is unnecessary for catalysis, and the absence of water-induced current enhancements supports the hypothesis of H_2O assisting in the delivery of protons when endo and exo protonation sites are distinct. As with the active site of [FeFe]-hydrogenase, the inclusion of a secondary amine functionality in $[Ni(7P^R_2N^H)_2]^{2+}$ ensures either endo or exo protonation leads to intermediates with suitably positioned protons (Figure 1).

CONCLUSION

We have reported the synthesis of $[Ni(7P^{Ph}_2N^H)_2H]^{3+}$, a new member of the $[Ni(7P^{Ph}_2N^{R'})_2]^{2+}$ family, and evaluated it for the electrocatalytic production of H_2. The complex is an active electrocatalyst under buffered acidic conditions with pK_a values ranging from 10−13, with turnover frequencies between 160 and 770 s^{-1} and overpotentials between 320 and 470 mV measured at $E_{cat/2}$. Studies of this complex yield mechanistic insights into the protonation steps of the catalytic cycle for H_2 production by $[Ni(7P^{Ph}_2N^{R'})_2]^{2+}$ catalysts. The use of a secondary amine as the proton relay eliminates the distinction between the exo- and endo-protonated isomers. Other members of the $[Ni(7P^{Ph}_2N^R)_2]^{2+}$ and $[Ni(P^{Ph}_2N^R_2)_2]^{2+}$ families showed substantial catalytic rate enhancements upon addition of H_2O, which was attributed to increasing the rate of endo protonation relative to nonproductive exo protonation. In the case of catalysis with in situ generated $[Ni(7P^{Ph}_2N^H)_2]^{2+}$, no water effect is observed, indicating that the beneficial effects from the addition of water have been eliminated. These findings are being used in our ongoing efforts to design H_2 production catalysts with faster rates and lower overpotentials through rational ligand modification based on a detailed mechanistic understanding.

MATERIALS AND METHODS

General Considerations. All manipulations with phosphine ligands and metal reagents were carried out under N_2 using standard vacuum line, Schlenk, and inert-atmosphere glovebox techniques. Solvents were purified by passage through neutral alumina using an Innovative Technology, Inc., PureSolv solvent purification system. The $[Ni(CH_3CN)_6](BF_4)_2$ was prepared according to literature procedures.[28] Ferrocene was purchased from Aldrich and sublimed under vacuum before use. Tetrabutylammonium hexafluorophosphate (Bu_4NPF_6) was purchased from the Tokyo Chemical Industry (TCI) and recrystallized three times from absolute ethanol. H_2O was purified using a Millipore Milli-Q purifier and was sparged with nitrogen before use.

NMR. NMR spectra were recorded on a Varian Inova spectrometer (500 MHz for ^1H) at 22 °C unless otherwise noted. All ^1H chemical shifts have been internally calibrated to the monoprotio impurity of the deuterated solvent. All $^{13}C\{^1H\}$ chemical shifts have been internally calibrated to the carbon atoms of the deuterated solvent. The $^{31}P\{^1H\}$ NMR spectra were referenced to external phosphoric acid at 0 ppm. The ^{19}F NMR spectra were referenced to external $CFCl_3$ at 0 ppm.

Electrochemistry. All experimental procedures were conducted at ambient temperature (22 °C) under nitrogen using a Vacuum Atmospheres drybox. A standard three-electrode configuration was employed in conjunction with a CH Instruments potentiostat interfaced to a computer with CH Instruments 700 D software. All voltammetric scans were recorded using glassy-carbon working electrode disks of 1 mm diameter (Cypress Systems EE040). Precise active electrode surface areas were determined by chronoamperometric measurements of ferrocene in 0.1 M Bu_4NPF_6/CH_3CN, using a diffusion coefficient of 2.4×10^{-5} cm^2 s^{-1}. The working electrode was treated between scans by means of a sequence of polishing with diamond paste (Buehler) of decreasing sizes (3 to 0.25 μm) interspersed by washings with purified H_2O. A glassy-carbon rod (Structure Probe, Inc.) was used as the auxiliary electrode. A frit-separated AgCl-coated Ag wire in 0.1 M Bu_4NPF_6/CH_3CN was used as the reference electrode. All glassware for electrochemical experiments was oven-dried overnight and cooled to room temperature before use. Ferrocene was used as an internal standard, and all potentials reported within this work are referenced to the $Cp_2Fe^{+/0}$ couple at 0 V. Controlled-potential electrolyses were performed using a CH Instruments 1100A power potentiostat, and gas analysis for H_2 was performed using an Agilent 6850 gas chromatograph equipped with a thermal conductivity detector fitted with a 10 ft long Supelco 1/8 in. Carbosieve 100/120 column and calibrated with two $H_2/N_2/CO/CO_2$ mixtures of known composition.

Synthesis of $7P^{Ph}_2N^{CHPh_2}$. Inside the glovebox, a Schlenk flask was charged with 1,2-bis(phenylphosphino)ethane

DOI: 10.1021/cs502132y
ACS Catal. 2015, 5, 2116−2123

(2.0 g; 8.12 mmol) and paraformaldehyde (0.530 g; 17.6 mmol). The reaction mixture was heated to 90 °C for 2 h, during which time the suspension turned clear and homogeneous. The reaction mixture was cooled, CH_3CN (25 mL) followed by benzyhydrylamine (1.4 mL; 1.48 g; 8.12 mmol) was added via syringe, and this mixture was heated to 70 °C for 2 h, upon which a white precipitate formed. All volatiles were removed in vacuo to yield a white solid consisting of the *meso* and *rac* isomers in an approximate 1/1 ratio (3.28 g, 7.23 mmol; 89% yield). The white solid was recrystallized twice from hot CH_3CN, yielding an analytically pure compound (2.55 g, 5.62 mmol; 69% yield). $^{31}P\{^1H\}$ NMR (CD_3CN, ppm): −38.9 (s, *meso*), −40.1 (s, *rac*). $^{13}C\{^1H\}$ NMR (CD_3CN, ppm): 137−128 (multiple peaks, *Ph*), 65.3 and 63.1 (s, *meso*/*rac*, N−$CH(C_6H_5)_2$), 49.3 and 45.6 (d, *meso*/*rac*, PCH_2N, J_{CP} = 13 Hz), 28.2−25.3 (multiple peaks, PCH_2CH_2P). ^1H NMR (CD_3CN, ppm): *meso* 7.54−7.17 (multiple peaks, 20H, P-C_6H_5 and N-$CH(C_6H_5)_2$), 4.98 (s, 1H, N-$CH(C_6H_5)_2$), 3.73−3.68 (mult, 2H, PCH_2N), 3.20−3.18 (mult, 2H, PCH_2N), 2.47−2.25 (mult, 4H, PCH_2CH_2P); *rac* 7.65−7.12 (multiple peaks, 20H, P-C_6H_5 and N-$CH(C_6H_5)_2$), 5.63 (s, 1H, N-$CH(C_6H_5)_2$), 3.49−3.26 (mult, 4H, PCH_2N), 2.50−2.19 (mult, 4H, PCH_2CH_2P). Anal. Calcd for $C_{29}H_{29}NP_2$ ($7P^{Ph}{}_2N^{CHPh_2}$): C, 76.81; H, 6.45; N, 3.09. Found: C, 76.55; H, 6.23; N, 2.85.

Synthesis of $[Ni(7P^{Ph}{}_2N^{CHPh_2})_2](BF_4)_2$. Inside the glovebox, a blue solution of $[Ni(MeCN)_6](BF_4)_2$ (0.241 g; 0.5 mmol) in CH_3CN (3 mL) was added to a suspension of $7P^{Ph}{}_2N^{CHPh_2}$ (0.453 g; 1.0 mmol) in CH_3CN (10 mL). An immediate color change to reddish brown was observed, and the reaction mixture was stirred at 22 °C for 3 h. The reaction mixture was filtered through Celite. All volatiles were removed in vacuo, and Et_2O was added to precipitate a reddish-brown solid. The solid was purified via vapor diffusion of Et_2O into a saturated CH_3CN solution to yield reddish-brown crystals (0.415 g; 0.364 mmol; 73% yield). The reddish-brown crystals were placed under vacuum (~1 × 10^{-4} mmHg) at 50 °C, yielding analytically pure compound. $^{31}P\{^1H\}$ NMR (CD_2Cl_2, ppm): 44.5 (s). ^{19}F NMR (CD_2Cl_2, ppm): −151.4 (s, BF_4^-). $^{13}C\{^1H\}$ NMR (CD_2Cl_2, ppm): 143−129 (multiple peaks, *Ph*), 69.2 (s, N−$CH(C_6H_5)_2$), 48.3 (d, PCH_2N, J_{CP} = 11 Hz), 31.3 (mult, PCH_2CH_2P). ^1H NMR (CD_2Cl_2, ppm): 7.41−6.87 (multiple peaks, 40H, P-C_6H_5 and N-$CH(C_6H_5)_2$), 4.97 (s, 2H, −$CH(C_6H_5)_2$), 3.90 (mult, 4H, PCH_2N), 3.28 (mult, 4H, PCH_2N), 3.15 (mult, 4H, PCH_2CH_2P), 2.51 (mult, 4H, PCH_2CH_2P). Anal. Calcd for $C_{58}H_{58}B_2F_8N_2NiP_4$ ($[Ni(7P^{Ph}{}_2N^{CHPh_2})_2](BF_4)_2$): C, 61.15; H, 5.13; N, 2.46. Found: C, 60.79; H, 5.27; N, 2.83. CV (0.2 M Bu_4NPF_6 in CH_3CN, scan rate 100 mV/s): $E_{1/2}$, V vs $Fc^{+/0}$ (ΔE_p, mV) −1.15 (93).

Synthesis of $[Ni(7P^{Ph}{}_2N^{H})_2H](BF_4)_3$ (Deprotection of N−H). A Schlenk flask was charged with $[Ni(7P^{Ph}{}_2N^{CHPh_2})_2](BF_4)_2$ (0.520 g; 0.456 mmol) in CH_2Cl_2 (20 mL). Under nitrogen, fresh $HBF_4{\cdot}Et_2O$ (0.236 g; 1.45 mmol) was added to the reaction mixture dropwise. Freshly opened $HBF_4{\cdot}Et_2O$ is required; otherwise, the reaction does not proceed cleanly enough to yield the desired product. A yellow precipitate immediately forms. The precipitate was isolated quickly on a frit and washed with Et_2O to afford a yellow solid (0.265 g; 0.296 mmol; 65% yield). The solid was dried under vacuum (~1 × 10^{-4} mmHg) at 50 °C for 24 h, yielding an analytically pure compound. $^{31}P\{^1H\}$ NMR (CD_3CN, ppm): 56.6 (br s), 47.7 (s), 45.7 (s). ^{19}F NMR (CD_3CN, ppm): −156.2 (s, BF_4^-). $^{13}C\{^1H\}$ NMR (CD_3CN, ppm): 148−132 (multiple peaks, some broad, *Ph*), 52.3 (d, PCH_2N, J_{CP} = 12 Hz), 34.3 (mult, PCH_2CH_2P). ^1H NMR (CD_3CN, ppm): 7.40 (overlapping m, 20H, Ar-*H*); 4.30−3.64 (multiple peaks, 8H, PCH_2N), 2.80−2.55 (multiple peaks, 8H, PCH_2CH_2P). Anal. Calcd for $C_{32}H_{39}B_3F_{12}N_2NiP_4$ ($[Ni(7P^{Ph}{}_2N^{H})_2H](BF_4)_3$): C, 42.96; H, 4.39; N, 3.13. Found: C, 42.89; H, 4.48; N, 3.18.

Catalytic Hydrogen Production using $[Ni(7P^{Ph_2}N^{H})_2H](BF_4)_3$ as Catalyst under Buffered Conditions. Typical Experimental Conditions. $[Ni(7P^{Ph}{}_2N^{H})_2H](BF_4)_3$ (1.7 mg, 0.0019 mmol), Bu_4NPF_6 (77.5 mg; 0.200 mmol), and ferrocene (0.4 mg, 0.002 mmol) were weighed into an 4 mL glass vial and dissolved in 2 mL of CH_3CN. The resulting mixture consists of 0.1 mM $[Ni(7P^{Ph}{}_2N^{H})_2H](BF_4)_3$ and 0.1 M $(Bu_4N)(PF_6)$. To this solution was added 5 μL of a 1.68 M Et_3N solution in CH_3CN via volumetric microsyringe. $[Ni(7P^{Ph}{}_2N^{H})_2H](BF_4)_3$ is a protonated species, and the addition of Et_3N is required to obtain a reversible cyclic voltammogram (i_p) prior to acid additions. In a separate vial, 1/1 stock/buffer solutions were prepared from 2,6-di-*tert*-butyl-4-methylpyridinium tetrafluoroborate (pK_a^{MeCN} = 12.8) and 2,6-di-*tert*-butyl-4-methylpyridine, anisidinium tetrafluoroborate (pK_a^{MeCN} = 11.86) and anisidine, 2,6-di-*tert*-butyl-pyridinium tetrafluoroborate (pK_a^{MeCN} = 11.4) and 2,6-di-*tert*-butylpyridinium, and anilinium tetrafluoroborate (pK_a^{MeCN} = 10.62) and aniline. The buffer components were dissolved in minimal CH_3CN (0.2 or 0.8 mL depending on solubility). The buffered solution was transferred to the electrochemical solution by volumetric microsyringe in a 10−50 μL aliquots. After each addition of buffer solution the working electrode was polished and rinsed (vide supra) and a cyclic voltammogram was recorded. The catalytic current (i_{cat}) was selected as the plateau of the wave as defined by second-derivative analysis.[27] After the completion of buffer solution additions, the described method was repeated using purified H_2O added via volumetric microsyringe in 5 μL increments up to 50 μL.

Controlled-Potential Coulometry. The bulk electrolysis vessel and its electrode were assembled under a flow of nitrogen. The working electrode consisted of a copper wire attached to a reticulated vitreous carbon cylinder, the reference electrode was a silver wire, and the auxiliary electrode was a nichrome wire; each was placed in a glass electrode compartment separated by Vycor frits. The total volume of this setup was determined to be 295 mL. Inside the glovebox, an electrolyte stock solution consisting of 0.1 M Bu_4NBF_4 in CH_3CN was prepared. This electrolyte stock solution was used to prepare a 25 mL solution consisting 0.89 mM $[(Ni(P^{Ph}{}_2N^{H})_2H](BF_4)_3$ (20.0 mg, 0.022 mmol) and ferrocene. This solution was transferred to the bulk electrolysis vessel, and a cyclic voltammogram was recorded. An acid solution containing 5 mL of electrolyte solution and collidinium tetrafluoroborate (707 mg; 3.38 mmol) was prepared inside the glovebox and added by syringe to the bulk electrolysis vessel. The final solution volume was 30 mL, consisting of 0.1 M Bu_4NBF_4, 0.73 mM $[(Ni(P^{Ph}{}_2N^{H})_2H](BF_4)_3$, and 0.11 M collidinium tetrafluoroborate and ferrocene. The controlled-potential coulometry was performed at −1.40 V versus ferrocenium/ferrocene as an internal reference. After 40.1, 60.2, and 80.3 C of charge had passed, a 1.0 mL sample of the headspace that had a total volume of 265 mL was removed via gastight syringe and analyzed by gas chromatography. Using the moles of H_2 produced and the charge passed, an average current efficiency of 95 ± 5% was calculated for H_2 production. Data are reported in Table S7 in the Supporting Information.

pK_a Determination for 2,6-Di-*tert*-butyl-4-methylpyridinium Tetrafluoroborate. Under an N_2 atmosphere, 2,6-di-*tert*-butyl-4-methylpyridinium tetrafluoroborate (40.0 mg; 0.136 mmol) was placed in a 1.0 mL volumetric flask and

DOI: 10.1021/cs502132y
ACS Catal. 2015, 5, 2116−2123

diluted to 1.0 mL with CD_3CN to yield a 0.136 M solution. In a second volumetric flask, *p*-anisidine (21.3 mg; 0.173 mmol) was diluted to 1.0 mL with CD_3CN to result in a 0.173 M solution. Five combinations of the acid and base solution were prepared in 1/4, 1/2, 1/1, 2/1, and 4/1 ratios. Analyzing these mixtures via ^1H NMR spectroscopy resulted in a pK_a value of 12.8 ± 0.2.

■ ASSOCIATED CONTENT

Supporting Information

The following files are available free of charge on the ACS Publications website at DOI: 10.1021/cs502132y.

Full experimental procedures (PDF)

X-ray crystallographic data (CIF)

■ AUTHOR INFORMATION

Corresponding Author

*E-mail for M.L.H.: monte.helm@pnnl.gov.

Notes

The authors declare no competing financial interest.

■ ACKNOWLEDGMENTS

We thank Daniel DuBois and Aaron Appel for helpful discussions and Ryan M. Stolley for collecting ^{13}C and ^{19}F NMR spectra. This research was supported as part of the Center for Molecular Electrocatalysis, an Energy Frontier Research Center funded by the U.S. Department of Energy, Office of Science, Office of Basic Energy Sciences. Pacific Northwest National Laboratory is operated by Battelle for the U.S. Department of Energy.

■ REFERENCES

(1) Lewis, N. S.; Nocera, D. G. *Proc. Natl. Acad. Sci. U.S.A.* **2006**, *103*, 15729−15735.

(2) Cook, T. R.; Dogutan, D. K.; Reece, S. Y.; Surendranath, Y.; Teets, T. S.; Nocera, D. G. *Chem. Rev.* **2010**, *110*, 6474−6502.

(3) McKone, J. R.; Marinescu, S. C.; Brunschwig, B. S.; Winkler, J. R.; Gray, H. B. *Chem. Sci.* **2014**, *5*, 865−878.

(4) Simmons, T. R.; Berggren, G.; Bacchi, M.; Fontecave, M.; Artero, V. *Coord. Chem. Rev.* **2014**, *270*−*271*, 127−150.

(5) Carroll, M. E.; Barton, B. E.; Rauchfuss, T. B.; Carroll, P. J. *J. Am. Chem. Soc.* **2012**, *134*, 18843−18852.

(6) DuBois, D. L. *Inorg. Chem.* **2014**, *53*, 3935−3960.

(7) Ginovska-Pangovska, B.; Dutta, A.; Reback, M. L.; Linehan, J. C.; Shaw, W. J. *Acc. Chem. Res.* **2014**, *47*, 2621−2630.

(8) Bullock, R. M.; Appel, A. M.; Helm, M. L. *Chem. Commun.* **2014**, *50*, 3125−3143.

(9) Fontecilla-Camps, J. C.; Volbeda, A.; Cavazza, C.; Nicolet, Y. *Chem. Rev.* **2007**, *107*, 4273−4303.

(10) Tard, C.; Pickett, C. J. *Chem. Rev.* **2009**, *109*, 2245−2274.

(11) Vincent, K. A.; Parkin, A.; Armstrong, F. A. *Chem. Rev.* **2007**, *107*, 4366−4413.

(12) Lubitz, W.; Ogata, H.; Rüdiger, O.; Reijerse, E. *Chem. Rev.* **2014**, *114*, 4081−4148.

(13) Frey, M. *ChemBioChem.* **2002**, *3*, 153−160.

(14) Crouthers, D. J.; Denny, J. A.; Bethel, R. D.; Munoz, D. G.; Darensbourg, M. Y. *Organometallics* **2014**, *33*, 4747−4755.

(15) Wiedner, E. S.; Roberts, J. A. S.; Dougherty, W. G.; Kassel, W. S.; DuBois, D. L.; Bullock, R. M. *Inorg. Chem.* **2013**, *52*, 9975−9988.

(16) Liu, T.; DuBois, D. L.; Bullock, R. M. *Nat. Chem.* **2013**, *5*, 228−233.

(17) Darmon, J. M.; Raugei, S.; Liu, T.; Hulley, E. B.; Weiss, C. J.; Bullock, R. M.; Helm, M. L. *ACS Catal.* **2014**, *4*, 1246−1260.

(18) Hulley, E. B.; Helm, M. L.; Bullock, R. M. *Chem. Sci.* **2014**, *5*, 4729−4741.

(19) Shaw, W. J.; Helm, M. L.; DuBois, D. L. *Biochim. Biophys. Acta, Bioenerg.* **2013**, *1827*, 1123−1139.

(20) Bullock, R. M. *Science* **2013**, *342*, 1054−1055.

(21) Helm, M. L.; Stewart, M. P.; Bullock, R. M.; Rakowski DuBois, M.; DuBois, D. L. *Science* **2011**, *333*, 863−866.

(22) Stewart, M. P.; Ho, M.-H.; Wiese, S.; Lindstrom, M. L.; Thogerson, C. E.; Raugei, S.; Bullock, R. M.; Helm, M. L. *J. Am. Chem. Soc.* **2013**, *135*, 6033−6046.

(23) O'Hagan, M. J.; Ho, M.-H.; Yang, J. Y.; Appel, A. M.; Rakowski DuBois, M.; Raugei, S.; Shaw, W. J.; DuBois, D. L.; Bullock, R. M. *J. Am. Chem. Soc.* **2012**, *134*, 19409−19424.

(24) O'Hagan, M. J.; Shaw, W. J.; Raugei, S.; Chen, S.; Yang, J. Y.; Kilgore, U. J.; DuBois, D. L.; Bullock, R. M. *J. Am. Chem. Soc.* **2011**, *133*, 14301−14312.

(25) Wuts, P. G. M.; Greene, T. W. In *Greene's Protective Groups in Organic Synthesis*; Wiley: Hoboken, NJ, USA, 2006; pp 696−926.

(26) Karasik, A. A.; Balueva, A. S.; Moussina, E. I.; Naumov, R. N.; Dobrynin, A. B.; Krivolapov, D. B.; Litvinov, I. A.; Sinyashin, O. G. *Heteroat. Chem.* **2008**, *19*, 125−132.

(27) Kilgore, U. J.; Roberts, J. A. S.; Pool, D. H.; Appel, A. M.; Stewart, M. P.; Rakowski DuBois, M.; Dougherty, W. G.; Kassel, W. S.; Bullock, R. M.; DuBois, D. L. *J. Am. Chem. Soc.* **2011**, *133*, 5861−5872.

(28) Kilgore, U. J.; Stewart, M. P.; Helm, M. L.; Dougherty, W. G.; Kassel, W. S.; Rakowski DuBois, M.; DuBois, D. L.; Bullock, R. M. *Inorg. Chem.* **2011**, *50*, 10908−10918.

(29) Nicholson, R. S.; Shain, I. *Anal. Chem.* **1964**, *36*, 706−723.

(30) Savéant, J. M. *Acc. Chem. Res.* **1980**, *13*, 323−329.

(31) Roberts, J. A. S.; Bullock, R. M. *Inorg. Chem.* **2013**, *52*, 3823−3835.

(32) Appel, A. M.; Helm, M. L. *ACS Catal.* **2014**, *4*, 630−633.

(33) Wiedner, E. S.; Yang, J. Y.; Chen, S.; Raugei, S.; Dougherty, W. G.; Kassel, W. S.; Helm, M. L.; Bullock, R. M.; Rakowski DuBois, M.; DuBois, D. L. *Organometallics* **2012**, *31*, 144−156.

(34) Kaljurand, I.; Rodima, T.; Leito, I.; Koppel, I. A.; Schwesinger, R. *J. Org. Chem.* **2000**, *65*, 6202−6208.

(35) Kaljurand, I.; Kütt, A.; Sooväli, L.; Rodima, T.; Mäemets, V.; Leito, I.; Koppel, I. A. *J. Org. Chem.* **2005**, *70*, 1019−1028.

(36) Kolthoff, I. M.; Chantooni, M. K.; Bhowmik, S. *Anal. Chem.* **1967**, *39*, 1627−1633.

(37) Izutsu, K. *Acid-Base Dissociation Constants in Dipolar Aprotic Solvents*; Blackwell Scientific: Oxford, U.K., 1990; p 21.

DOI: 10.1021/cs502132y
ACS Catal. 2015, 5, 2116−2123